ELSEVIER

Biophysical Chemistry 130 (2007) 114–121

Biophysical Chemistry

http://www.elsevier.com/locate/biophyschem

A comparative Mössbauer study of the mineral cores of human H-chain ferritin employing dioxygen and hydrogen peroxide as iron oxidants

Fadi Bou-Abdallah [a], Elissa Carney [b], N. Dennis Chasteen [a], Paolo Arosio [c], Arthur J. Viescas [b], Georgia C. Papaefthymiou [b,*]

[a] *Department of Chemistry, University of New Hampshire, Durham, NH 03824, United States*
[b] *Department of Physics, Villanova University, Villanova, PA 19085, United States*
[c] *Chemistry Section, Faculty of Medicine, University of Brescia, 25123 Brescia, Italy*

Received 18 June 2007; accepted 4 August 2007
Available online 22 August 2007

Abstract

Ferritins are ubiquitous iron storage and detoxification proteins distributed throughout the plant and animal kingdoms. Mammalian ferritins oxidize and accumulate iron as a ferrihydrite mineral within a shell-like protein cavity. Iron deposition utilizes both O_2 and H_2O_2 as oxidants for Fe^{2+} where oxidation can occur either at protein ferroxidase centers or directly on the surface of the growing mineral core. The present study was undertaken to determine whether the nature of the mineral core formed depends on the protein ferroxidase center versus mineral surface mechanism and on H_2O_2 versus O_2 as the oxidant. The data reveal that similar cores are produced in all instances, suggesting that the structure of the core is thermodynamically, not kinetically controlled. Cores averaging 500 Fe/protein shell and diameter ~2.6 nm were prepared and exhibited superparamagnetic blocking temperatures of 19 and 22 K for the H_2O_2 and O_2 oxidized samples, respectively. The observed blocking temperatures are consistent with the unexpectedly large effective anisotropy constant K_{eff}=312 kJ/m^3 recently reported for ferrihydrite nanoparticles formed in reverse micelles [E.L. Duarte, R. Itri, E. Lima Jr., M.S. Batista, T.S. Berquó and G.F. Goya, Large Magnetic Anisotropy in ferrihydrite nanoparticles synthesized from reverse micelles, Nanotechnology 17 (2006) 5549–5555.]. All ferritin samples exhibited two magnetic phases present in nearly equal amounts and ascribed to iron spins at the surface and in the interior of the nanoparticle. At 4.2 K, the surface spins exhibit hyperfine fields, H_{hf}, of 436 and 445 kOe for the H_2O_2 and O_2 samples, respectively. As expected, the spins in the interior of the core exhibit larger H_{hf} values, *i.e.* 478 and 486 kOe for the H_2O_2 and O_2 samples, respectively. The slightly smaller hyperfine field distribution DH_{hf} for both surface (78 kOe vs. 92 kOe) and interior spins (45 kOe vs. 54 kOe) of the O_2 sample compared to the H_2O_2 samples implies that the former is somewhat more crystalline.

Keywords: Mössbauer spectroscopy; Ferrihydrite; Ferritin; Iron oxidation; Hydrogen peroxide

1. Introduction

Ferritins are a family of iron storage and detoxification proteins present in animals, plants and microbes. The protein has a shell-like structure composed of 24 similar or identical subunits encapsulating a hydrous ferric oxide mineral core, the storage form of iron [1–4]. More recently, ferritin-like Dps proteins (*D*NA binding *p*rotein from *s*tarved cells) composed of only 12 subunits have been discovered in bacteria and likewise form mineral cores albeit of much smaller size, ~500 Fe/shell versus ~4500 Fe/shell for canonical ferritins [4–8]. The canonical ferritins and the Dps proteins have ferroxidase centers that initiate and/or sustain mineralization [1–11]. The ferroxidase centers of mammalian ferritins are located on H-type subunits whereas L-subunits appear to play a role in nucleation of the mineral core [11]. In human H-chain ferritin (HuHF), it is now recognized that there are

Abbreviations: HoSF, horse spleen ferritin; HuHF, recombinant human H-chain ferritin; Mops, 3-(*N*-morpholino)propanesulfonic acid.

* Corresponding author. Tel.: +1 610 519 4883; fax: +1 610 519 7465.
E-mail address: gcp@villanova.edu (G.C. Papaefthymiou).

0301-4622/$ - see front matter © 2007 Published by Elsevier B.V.
doi:10.1016/j.bpc.2007.08.003

three chemical pathways for developing the mineral core [12]. Eq. (1)

$$2Fe^{2+} + O_2 + 4H_2O \rightarrow 2Fe(O)OH_{(core)} + H_2O_2 + 4H^+ \quad (1)$$

$$2Fe^{2+} + H_2O_2 + 2H_2O \rightarrow 2Fe(O)OH_{(core)} + 4H^+ \quad (2)$$

$$4Fe^{2+} + O_2 + 6H_2O \rightarrow 4Fe(O)OH_{(core)} + 8H^+ \quad (3)$$

represents the overall reaction catalyzed by the 24 ferroxidase centers of the protein where Fe^{2+} is oxidized by O_2. The resultant Fe^{3+} is subsequently transferred to the mineral core. Much of the hydrogen peroxide produced in Eq. (1) reacts through Eq. (2), the detoxification reaction, which also occurs at the ferroxidase centers. Fe^{2+} is oxidized at the ferroxidase centers by both O_2 and H_2O_2 via Eqs. (1) and (2) at comparable rates [13]. The pairwise oxidation of two Fe^{2+} per H_2O_2 avoids the odd electron chemistry associated with hydroxyl radical production via the Fenton reaction and accounts for the detoxification properties of ferritin and its ability to protect cells from oxidative damage [14–17]. Once a sufficient core has been developed ($\geq$800 Fe/shell), Eq. (3) becomes the dominant reaction where Fe^{2+} is oxidized on the surface of the mineral in an autocatalytic fashion and O_2 is reduced completely to water [12]. In the case of Dps proteins from bacteria, H_2O_2 is the primary oxidant for Fe^{2+} at the ferroxidase centers of these proteins and the mineralization reaction proceeds according to Eq. (2) [7,8].

The structure of the ferritin core has been extensively reviewed [18–20]. It is generally agreed that the core is structurally similar to ferrihydrite, the structure of which has been recently determined [20]. The formula $Fe_{10}O_{14}(OH)_2$ for ferrihydrite in an ideal structure is abbreviated here as simply $Fe(O)OH_{(core)}$. Electron microscopy suggests that the core may be single crystalline or polycrystalline, nucleated at different points within the protein shell [19]. More recent electron nano-diffraction experiments with a 1 nm beam diameter indicate that each core contains a single phase, but different cores in the mix could contain different phases, some amorphous and some crystalline [21]. Thus, questions about the exact nature of the ferritin biomineralization product, its dependence on sample handling and detailed conditions of preparation remain. In nature, additional components, such as phosphates, add to the diversity of ferritin cores extracted from different sources [2,22]. In vitro reconstituted ferritin, however, is expected to be in the form of ferrihydrite. The majority of previous Mössbauer investigations have dealt with half to fully loaded ferritin cores (1000–4500 Fe/shell), with the very early stages of iron complexation with the protein (50 Fe/shell) or with small clusters that are precursors to more fully developed cores [23,24].

To date the Mössbauer properties of cores of intermediate size (500 Fe/shell) have not been investigated nor has there been a study addressing the structural and magnetic properties of cores formed with H_2O_2 versus O_2 as the oxidant. In addition, it is unknown whether there is a significant difference between cores generated via the ferroxidase reaction (Eqs. (1) and (2)) and the mineral surface reaction (Eq. (3)). In the present investigation we have examined HuHF at intermediate levels of iron loading, 500 Fe/protein shell on average, and evaluated the Mössbauer spectra of the nanoparticle cores formed with these two oxidants. The results reveal that similar cores are obtained whether Fe^{2+} is oxidized by O_2 or H_2O_2 and whether the core is produced from ferroxidase centered catalyzed iron oxidation or from autocatalytic oxidation of iron on the growing mineral surface. The cores obtained using either oxidant are composed of two magnetic phases, one corresponding to an iron interior to the mineral core (subsites 1) and the other to an iron at the surface of the core (subsites 2).

2. Materials and methods

Recombinant H-chain ferritin was prepared as previously described [25] and rendered iron free by anaerobic ultra filtration with dithionite and bipyridyl [26]. The H-chain concentration was determined by the absorbance at 280 nm using ε=23,000 M^{-1} cm^{-1} per subunit. Ferritin reconstitution was performed with 100% iron-57 enriched salts ($^{57}FeSO_4$). The final H-chain ferritin and iron concentrations were 20 μM and 0.01 M, respectively (500 Fe/shell), in an aqueous buffer solution of 0.15 M (sample #1) or 0.075 M (samples #2, 3, 4) Mops, pH 7.0. The oxidation of iron by H_2O_2 in HuHF was performed under anaerobic conditions using ultra high pure argon gas (99.995%, <5 ppm O_2). For sample #1, 12 μl of 0.5 M H_2O_2 was titrated into a 500 μl $^{57}Fe^{2+}$-HuHF solution in increments of 1 μl per addition corresponding to 0.1 H_2O_2/Fe(II) added each time to give a final ratio of ~1.2 H_2O_2/Fe(II). For samples #2 and #3, 220 μl ^{57}Fe (500 Fe/shell) was added at once to 220 μl HuHF solution in 21 or 100% O_2 and allowed to react overnight. For sample #4, 220 μl ^{57}Fe was added to 220 μl HuHF (100% O_2) in increments of 50 Fe(II)/shell for a total of 10 increments.

The $^{57}FeSO_4$ solution was prepared by dissolving 1.104 mg of ^{57}Fe metal (95.1 at.%; U.S. Service, Inc. Summit, NJ, USA) in 200 μl of 0.2 M H_2SO_4 (14% v/v) over a period of 3 days, followed by dilution with 750 μl water to produce a final solution of 20 mM $FeSO_4$, pH ~2.0.

A conventional transmission Mössbauer spectrometer was used. Sample temperature was varied in the range $4.2 \leq T \leq 120$ K, employing a continuous flow liquid He cryostat by Janis Corporation and a Lake Shore temperature controller. The source was ^{57}Co in Rh matrix maintained at room temperature. A 6 μm-thick iron foil enriched in ^{57}Fe was used for calibration. All isomer shifts are referenced to α-Fe at room temperature. Least-square fits to the experimental data were performed by a least-square fitting procedure to Lorentzian absorption lines, including distribution of hyperfine parameters.

3. Results and discussion

A comparative Mössbauer study of the ferritin iron cores formed upon oxidation in exclusively 100% O_2 atmosphere (~1.3 mM O_2 solution, sample #3) vs. ~12 mM H_2O_2 solution (sample #1) was carried out, over the temperature range of $4.2 \leq T \leq 120$ K. The complete Mössbauer spectral thermal

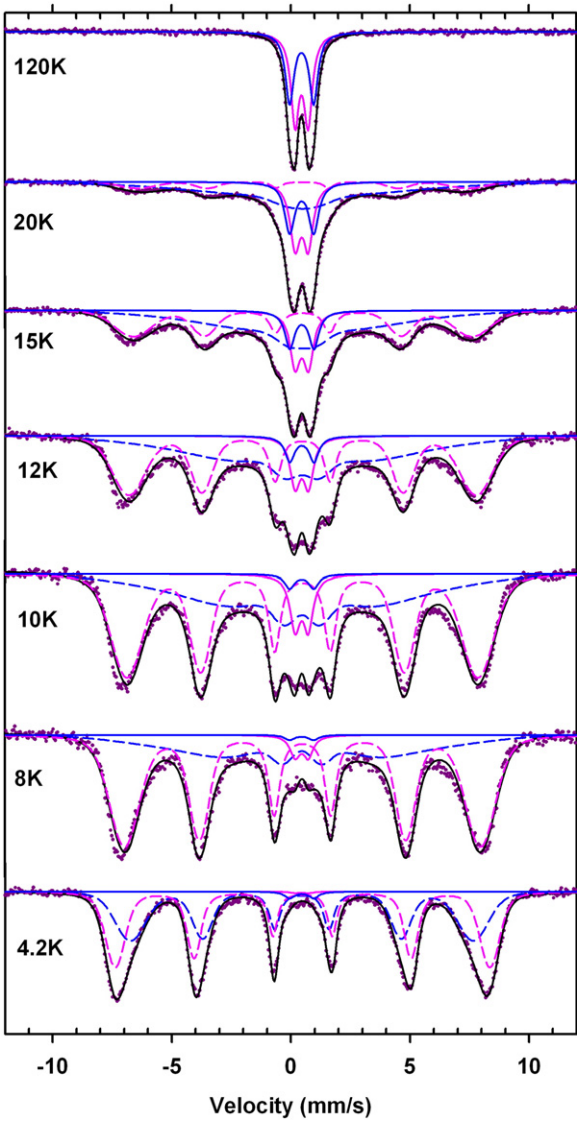

Fig. 1. Mössbauer spectra at various temperatures of HuHF (500 Fe/protein) oxidized with 100% oxygen atmosphere (sample #3). The solid lines through the experimental points are least-square fits to a superposition of quadrupolar and magnetic iron subsites as indicated by the simulated subspectra. The broken red and blue lines denote the spectra of magnetic subsites 1 and 2, respectively. Solid red and blue lines denote the corresponding quadrupolar subsites 1 and 2. A small amount of quadrupolar contributions are discernible down to 4.2 K. (For interpretation of the references to colour in this figure legend, the reader is referred to the web version of this article.)

profiles are presented in Figs. 1 and 2, while Fig. 3 shows the 4.2 K data with the associated hyperfine field distributions. Derived Mössbauer parameters are summarized in Table 1. The 4.2 K spectrum for a sample prepared with a 21% O_2 atmosphere (~0.28 mM solution, sample #2) is identical to that of the 100% O_2 sample (sample #3). It has been previously shown that the kinetics of iron oxidation saturates in rate at about 0.30 mM O_2 for the horse spleen protein [27].

The resulting iron core phases obtained with either O_2 or H_2O_2 as the oxidant for Fe^{2+} ions are very similar, as judged from their Mössbauer spectra, even though detailed examination reveals some differences. Similarly, whether Fe^{2+} is added to the protein in 10 increments of 50 Fe (sample #4) or 500 Fe at once (sample #3) with 100% O_2 as the oxidant produces cores that are indistinguishable at 4.2 K. The incremental addition of iron produces cores largely through the ferroxidase reaction 1 [9,12,27] whereas the single addition of 500 Fe produces cores that are generated by all three reactions (~40%, 28% and ~32% by Eqs. (1), (2) and (3), respectively) [12]. We conclude that the various core formation reactions utilizing O_2 or H_2O_2 as the oxidant, through the protein ferroxidase site or directly on the growing core, all lead to substantially the same mineral. This result was unexpected given the markedly different chemistries involved in producing the core by the three reactions. The

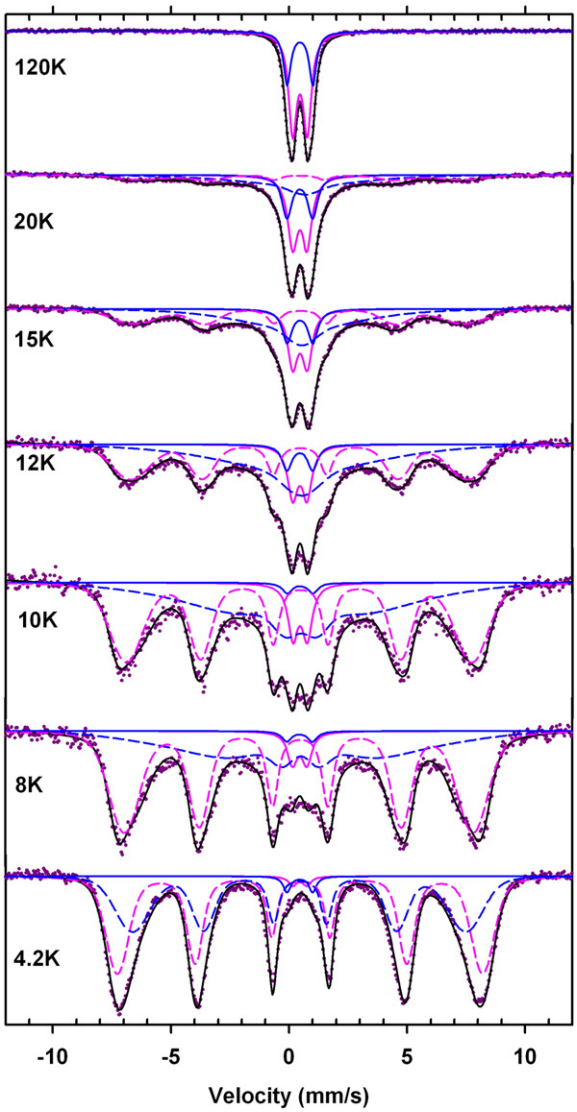

Fig. 2. Mössbauer spectra at various temperatures of HuHF (500 Fe/protein) oxidized with 12 mM hydrogen peroxide (sample #1). The solid lines through the experimental points are least-square fits to a superposition of quadrupolar and magnetic iron subsites as indicated by the simulated subspectra. The broken red and blue lines denote the spectra of magnetic subsites 1 and 2, respectively. Solid red and blue lines denote the corresponding quadrupolar subsites 1 and 2. A small amount of quadrupolar contributions are discernible down to 4.2 K. (For interpretation of the references to colour in this figure legend, the reader is referred to the web version of this article.)

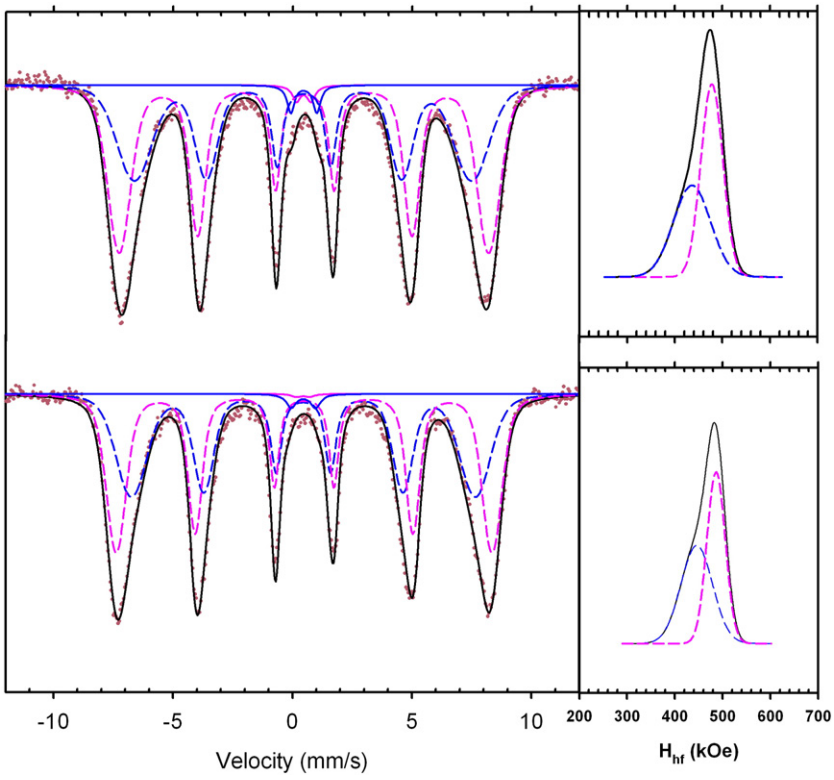

Fig. 3. Mössbauer spectra at 4.2 K for O_2 (sample #3, bottom) and H_2O_2 (sample #1, top) oxidized HuHF (500 Fe/protein) samples with associated hyperfine magnetic field distributions shown on the right. Color scheme for superimposed subspectra is same as in Figs. 1 and 2. (For interpretation of the references to colour in this figure legend, the reader is referred to the web version of this article.)

thermodynamic stability of the nanoparticle phase rather than kinetics appears to govern the final product in all cases.

The spectra with either O_2 or H_2O_2 conform to those of superparamagnetic ferrihydrite [28–31] with a blocking temperature around 20 K. Specific features include broad spectral absorption lines, characteristic of poor phase crystallinity, and asymmetrically broadened magnetic hyperfine absorption lines. In order to obtain least-squares fits with acceptable χ^2 values, experimental spectra required at least the superposition of two iron subsites, both in the collapsed superparamagnetic state seen at high temperature (120 K) and in the low temperature (4.2 K) magnetically split state. The quadrupolar spectra at 120 K were fit with the superposition of two doublets with similar isomer shifts but markedly different quadrupole splittings. Fitted Mössbauer

Table 1
Mössbauer parameters for HuHF, 500 Fe/protein

Sample	T (K)	Subsite	δ [a] (mm/s) ±0.03	ΔE_Q [b] (mm/s) ±0.05	Γ [c] (mm/s) ±0.03	$<H_{hf}>$ [d] (kOe)	DH_{hf} [e] (kOe)	Area [f] (%)±0.1
O_2 oxidized	120	1 (inner)	0.46	0.55	0.41	–	–	55.0
(sample #3)		2 (surface)	0.46	1.01	0.43	–	–	45.0
	4.2	1 (inner)	0.46	0.55	0.50	–	–	0.3
		2 (surface)	0.46	1.01	0.50	–	–	1.0
		1 (inner)	0.49	–	0.44	486	45	50.7
		2 (surface)	0.46	–	0.47	445	78	48.0
H_2O_2 oxidized	120	1 (inner)	0.46	0.59	0.41	–	–	59.0
(sample #1)		2 (surface)	0.46	1.04	0.43	–	–	41.0
	4.2	1 (inner)	0.46	0.61	0.42	–	–	1.0
		2 (surface)	0.46	1.09	0.43	–	–	2.0
		1(inner)	0.48	–	0.47	478	54	54.0
		2 (surface)	0.45	–	–	436	92	43.0

[a] Isomer shifts relative to metallic iron at room temperature.
[b] Quadrupole splitting.
[c] Full width at half height of the Lorentzian line.
[d] Hyperfine field.
[e] Full width at half maximum of hyperfine field distribution.
[f] Relative areas of the subspectra.

parameters for the O_2-oxidized sample #3 at $T=120$ K are $\delta_1=0.46$ mm/s, $\Delta E_{Q1}=0.55$ mm/s comprising 55% of absorption intensity; and $\delta_2=0.46$ mm/s and $\Delta E_{Q2}=1.01$ mm/s comprising 45% of absorption intensity. The corresponding parameters for the H_2O_2-oxidized sample are: $\delta_1=0.46$ mm/s, $\Delta E_{Q1}=0.59$ mm/s comprising 59% of absorption intensity and $\delta_2=0.46$ mm/s and $\Delta E_{Q2}=1.04$ mm/s comprising 41% of absorption intensity. The large quadrupole splittings for high spin Fe^{3+} sites observed at the surface point to severely distorted iron coordination at the surface compared to the interior.

At 4.2 K the magnetically split spectra also required the superposition of two magnetic subsites 1 and 2 (depicted in broken red and blue lines in Figs. 1 and 2) with broad hyperfine field distributions, shown in Fig. 3. Average hyperfine fields of $<H_{hf}>_1=486$ kOe and $<H_{hf}>_2=445$ kOe for the O_2-oxidized sample, and $<H_{hf}>_1=478$ kOe and $<H_{hf}>_2=436$ kOe for the H_2O_2-oxidized sample were obtained. Minority components of quadrupolar doublets are still discernable at 4.2 K, (shown in solid red and blue lines) comprising less than 2% of total absorption area for both O_2 and H_2O_2 samples (Table 1). These observations all point to some heterogeneity in the cores, both in size and degrees of crystallinity, consistent with previous observations with ferritins of different types [32,33]. The broader hyperfine field distributions DH_{hf} seen for both spectral subcomponents of the H_2O_2 sample compared to the O_2 sample in Fig. 3 suggests greater heterogeneity (lower crystallinity) in the former. Values for the field distributions DH_{hf} are given in Table 1.

Magnetic subcomponent 1 (broken red line in Figs. 1 and 2 for O_2 and H_2O_2 samples, respectively) exhibits slow-spin-relaxation up to 20 K, before collapsing to a quadrupolar doublet; in contrast, subcomponent 2 is grossly broadened, consistent with intermediate-spin-relaxation. Fig. 4 shows the temperature dependence of the fraction of magnetic to total spectral absorption area, f, for the H_2O_2 and O_2 samples. The solid lines through the data points are least-square fits to sigmoidal curves. Operationally, the blocking temperature for a distribution of particle sizes is defined as the temperature at which $f=0.5$. This determines $T_B=19$ K and 22 K for H_2O_2- and O_2-oxidized proteins respectively, indicated by the arrows in Fig. 4. The observed blocking temperatures are much lower than the average blocking temperature for horse spleen ferritin containing an average of ~3000 Fe/shell, namely $<T_B>=38$ K [34]. As would be expected, this result indicates that at 500 Fe/shell the average core size is smaller than the fully loaded ferritin cores of 8 nm diameter containing ~4500 Fe [35].

The observed temperature dependence of the magnetic fraction as the sample goes through the blocking temperature contains information on the particle size distribution in the sample, through the temperature dependence of the derivative df/dT [36]. The superparamagnetic relaxation time, τ_s, is governed by Eq. (4) where τ_0 is a constant

$$\tau_s = \tau_0 \exp\left(K_{eff} V / k_B T\right) \quad (4)$$

characteristic of the material, K_{eff} is the effective magnetic anisotropy density, k_B is Boltzmann's constant and T is the temperature [37–39]. At a certain temperature particles smaller

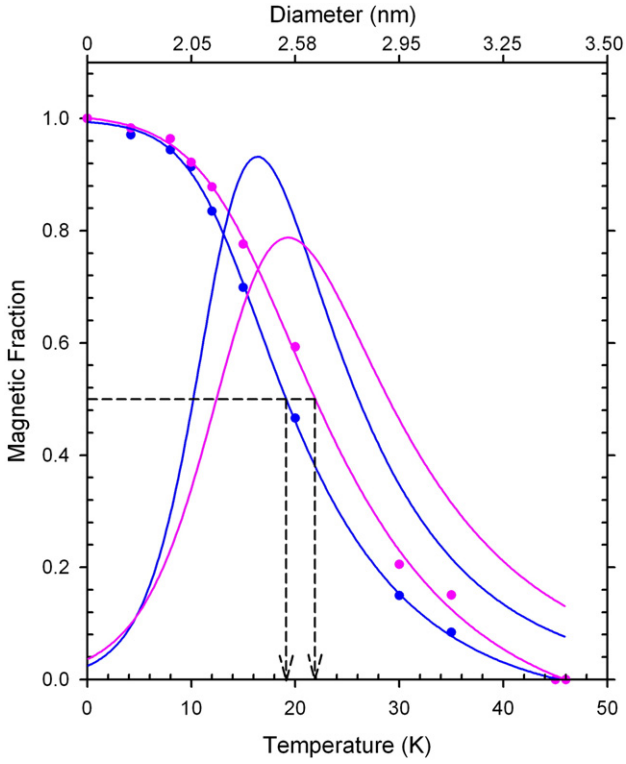

Fig. 4. Magnetic fraction, f, showing sigmoidal temperature dependence, for O_2- (red, sample #3) and H_2O_2-oxidized (blue, sample #1) HuHF 500 Fe/protein. The blocking temperatures are indicated by the arrows, T_B (O_2-oxidized)=22 K and T_B (H_2O_2-oxidized)=19 K. Bell shaped curves give derived particle size distributions as indicated on top horizontal scale. (For interpretation of the references to colour in this figure legend, the reader is referred to the web version of this article.)

than a critical size are superparamagnetic, while those larger than this size are magnetically blocked, and thus, contribute to the magnetic fraction of the Mössbauer spectrum. At the blocking temperature, the relaxation time becomes equal to τ_L, the Larmor precession time of the ^{57}Fe-nuclear spin in its excited state, in the effective field at the nucleus. Using $\tau_L=2.5\times10^{-8}$ s, $\tau_0=10^{-12}$ s, previously determined for ferritin [40], and $K_{eff}=312$ kJ/m^3 as recently determined for the ferrihydrite nanoparticles in reverse micelles [28], we can map blocking temperature to particle size, as indicated in Fig. 4 (top axis). The blocking temperatures of 22 and 19 K correspond to the average particle size of ~2.66 and ~2.53 nm diameter for the O_2- and H_2O_2-oxidized proteins, respectively. These values compare favorably with the average core size of 2.6±0.8 nm ($N=100$) recently reported for HoSF to which 500 Fe had been added to the apoprotein and the core size distribution measured by transmission electron microscopy [41]. It is noteworthy that the anisotropy constant K_{eff} determined for micelles is about 50 times larger than the value of $K_{eff}=6.7$ kJ/m^3 previously measured on ferritins containing an average of 1730–2480 Fe/shell [35]. Contributions other than the magnetocrystalline anisotropy of the bulk become dominant in small particles resulting from surface, shape and strain anisotropies [34].

Investigation of the properties of small magnetically ordered particles has been an active area of research for a number of years. Significant contributions by the Mössbauer community

have elucidated small particle magnetism of iron containing systems in general, and the iron biomineral core of ferritin, in particular. It is generally agreed that surface atoms have distorted coordination relative to inner, core atoms, leading to larger quadruple splitting, spin canting and significantly reduced hyperfine magnetic fields at the surface relative to inner core atoms [42–45]. In experimental studies, including transmission Mössbauer spectroscopy, the surface contribution to the spectral profile becomes increasingly observable as the average particle size decreases. Thus, for these exceptionally small ferrihydrite particles, it is reasonable to associate the two spectral components observed to inner core vs. surface iron atoms, as previously proposed specifically for the ferritin iron core, based on water proton T_2 relaxometry studies [46]. For a spherical core, the number of surface Fe atoms n_S is related to the total Fe in the core n_T by the relationship $n_S = 4 \cdot n_T^{2/3}$ [47]. For a core of $n_T = 500$ Fe, we calculate $n_S = 252$, corresponding to about 50% of the iron being at the surface. This value is comparable to the percentages derived from fitting of the Mössbauer spectra (Table 1) and argues for cores of 500 Fe/shell size being approximately spherical in shape in HuHF. In the case of HoSF (500 Fe/shell) the cores are irregular in shape [41]; however, ultracentrifugation studies of HoSF and HuHF show that HuHF used here produces cores of much more uniform size [48], an observation pointing to the importance of the protein shell and its associated ferroxidase and nucleation sites in governing the nature of the core particle obtained. More complicated geometries are likely present in larger core particles and are dependent on sample preparation and represent a larger percentage of Fe being on the surface relative to a spherical particle as discussed elsewhere [47].

Fig. 5 gives a plot of the average hyperfine magnetic field values, obtained from the least-square fits to distributions of magnetic hyperfine fields, with respect to temperature. The temperature dependence of the hyperfine field associated with inner sites is consistent with the theory of collective magnetic excitations of Mørup and Topsøe [49], according to which precession of the particle's magnetization about the anisotropy axis, at temperatures insufficient to induce a full spin-flip and therefore superparamagnetic relaxation, results in a slight diminution of the recorded hyperfine field. A linear decrease of the hyperfine field is predicted according to $H_{hf}(T) = H_{hf}^0(1 - k_B T/2K_{eff}V)$, where H_{hf}^0 is the saturated hyperfine field at 0 K. A maximum decrease in the value of the field of about 15% from saturation is expected through this process. In contrast, subcomponent 2 exhibits a marked decrease in hyperfine field values with increasing temperature. This observation is consistent with theories of many-spin nano-magnet systems, where surface anisotropies introduce spin canting and a greater complexity in the potential energy landscape that supports low energy spin-wave excitations and produces steps and minor hysteresis loops in the SQUID magnetization measurements [50]. Characteristically, a similar deviation in behavior is predicted in theoretical calculations of a many-spin cluster system [51] for the inner versus surface local magnetization, σ, which is proportionally related to the local hyperfine field. As the Larmor precession time, τ_L, of the ^{57}Fe nuclear spin is proportional the local hyperfine field, the surface spins enter an intermediate relaxation regime prior to $T = 20$ K; in contrast, at 20 K the inner spins undergo a slow to fast spin relaxation transition, for the characteristic Mössbauer measuring time of $\sim 10^{-8}$ s, when thermal energy overcomes the potential barrier, $K_{eff}V$, and the particle becomes superparamagnetic.

The surface hyperfine fields associated with the H_2O_2-oxidized protein exhibit a sharper decrease with increasing temperature (Fig. 5, blue dots) compared to those of O_2-oxidized protein (Fig. 5, red triangles); while the hyperfine fields associated with inner iron sites exhibit similar temperature dependence, independent of the nature of the oxidant. This would indicate that the two types of cores must differ in some minor characteristics at their surface, where unpassivated, daggling free bonds contribute positive Gibbs free energy to the particle.

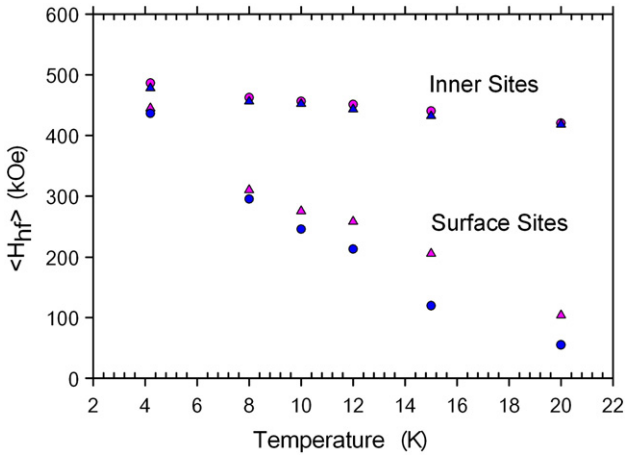

Fig. 5. Temperature dependence of the average hyperfine fields at inner and surface iron sites for O_2 (red, sample #3) and H_2O_2 (blue, sample #1) oxidized HuHF 500 Fe/protein. (For interpretation of the references to colour in this figure legend, the reader is referred to the web version of this article.)

4. Conclusion

In summary, Mössbauer measurements have been made for the first time on ferritin cores of intermediate size (500 Fe/shell) using both H_2O_2 and the more conventional oxidant O_2 employed in previous studies. Significantly, the cores generated are independent of the oxidant employed, the partial pressure of O_2 used and the reaction pathway (Eqs. (1), (2) or (3)). A consistent picture emerges of the nanoparticle core, one of approximately spherical shape of diameter ~2.6 nm with 50% of the Fe residing on the surface. The magnetic properties of surface iron likely contribute significantly to T_2 relaxation enhancement in proton magnetic resonance images of iron loaded tissues [46]. The observed blocking temperatures support the notion that smaller iron oxide nanoparticles can have significantly larger effective anisotropy constants K_{eff}.

Acknowledgement

This research was supported by NIH grant R01GM20194 (NDC) and by NSF grant DMR-0604049 (GCP).

References

[1] E.C. Theil, M. Matzapetakis, X. Liu, Ferritins: iron/oxygen biominerals in protein nanocages, JBIC 11 (2006) 803–810.

[2] N.D. Chasteen, P.M. Harrison, Mineralization in ferritin: an efficient means of iron storage, J. Struct. Biol. 126 (1999) 182–194.

[3] S.C. Andrews, A.K. Robinson, F. Rodríguez-Quiñones, Bacterial iron homeostasis, FEMS Microbiol. Rev. 27 (2003) 215–237.

[4] J.L. Smith, The physiological role of ferritin-like compounds in bacteria, Crit. Rev. Microbiol. 30 (2004) 173–185.

[5] E. Chiancone, P. Ceci, A. Ilari, F. Ribacchi, S. Stefanini, Iron and proteins for iron storage and detoxification, BioMetals 17 (2004) 197–202.

[6] M. Su, S. Cavallo, S. Stefanini, E. Chiancone, N.D. Chasteen, The so-called *Listeria innocua* ferritin is a Dps protein. Iron incorporation, detoxification and DNA protection properties, Biochemistry 44 (2005) 5572–5578.

[7] G. Zhao, P. Ceci, A. Ilari, L. Giangiacomo, T.M. Laue, E. Chiancone, N.D. Chasteen, Iron and hydrogen peroxide detoxification properties of DNA-binding protein from starved cells. A ferritin-like DNA-binding protein of *Escherichia coli*, J. Biol. Chem. 277 (2002) 27689–27696.

[8] A. Ilari, S. Stefanini, E. Chiancone, D. Tsernoglou, The dodecameric ferritin from *Listeria innocua* contains a novel intersubunit iron-binding site, Nat. Struct. Biol. 7 (2000) 38–43.

[9] F. Bou-Abdallah, G. Zhao, H.R. Mayne, P. Arosio, N.D. Chasteen, Origin of the unusual kinetics of iron deposition in human H-Chain ferritin, J. Am. Chem. Soc. 127 (2005) 3885–3893.

[10] A. Ilari, M.C. Latella, P. Ceci, F. Ribacchi, M. Su, L. Giangiacomo, S. Stefanini, N.D. Chasteen, E. Chiancone, The unusual intersubunit ferroxidase center of *Listeria innocua* Dps is required for hydrogen peroxide detoxification but not for iron uptake. A study with site-specific mutants, Biochemistry 44 (2005) 5579–5587.

[11] P.M. Harrison, P. Arosio, Ferritins: molecular properties, iron storage function and cellular regulation, Biochim. Biophys. Acta 1275 (1996) 161–203.

[12] G. Zhao, F. Bou-Abdallah, P. Arosio, S. Levi, C. Janus-Chandler, N.D. Chasteen, Multiple pathways for mineral core formation in mammalian apoferritin. The role of hydrogen peroxide, Biochemistry 42 (2003) 3142–3150.

[13] J. Bunker, T. Lowry, G. David, B. Zhang, D. Brosnahan, S. Lindsay, R. Costen, S. Choi, P. Arosio, G.D. Watt, Kinetics of iron deposition catalyzed by recombinant human liver heavy and light ferritins and *Azotobacter vinelandii* bacterioferrin using O_2 and H_2O_2 as oxidants, Biophys. Chem. 114 (2005) 235–244.

[14] G. Zhao, P. Arosio, N.D. Chasteen, Iron(II) and hydrogen peroxide detoxification properties of human H-chain ferritin. An EPR spin-trapping study, Biochemistry 45 (2006) 3429–3436.

[15] A. Cozzi, B. Corsi, S. Levi, P. Santambrogio, A. Albertini, P. Arosio, Overexpression of wild type and mutated human ferritin H-chain in HeLa cells: *in vivo* role of ferritin ferroxidase activity, J. Biol. Chem. 275 (2000) 25122–25129.

[16] S. Epsztejn, H. Glickstein, V. Picard, I.N. Slotki, W. Breuer, C. Beaumont, Z.I. Cabantchik, H-ferritin subunit overexpression in erythroid cells reduces the oxidative stress response and induces multidrug resistance properties, Blood 94 (1999) 3593–3603.

[17] K.J. Thompson, M.G. Fried, Z. Ye, P. Boyer, J.R. Connor, Regulation, mechanisms and proposed function of ferritin translocation to cell nuclei, J. Cell Sci. 115 (2002) 2165–2177.

[18] T.G. St. Pierre, J. Webb, S. Mann, Biomineralization: chemical and biochemical perspectives, in: S. Man, J. Webb, R.J.P. Williams (Eds.), Ferritin and Hemosiderin: Structural and Magnetic Studies of the Iron Core, VCH, Weinheim, Germany, 1989, p. 295.

[19] W.H. Massover, Ultrastructure of ferritin and apoferritin: a review, Micron 24 (1993) 389–437.

[20] F.M. Michel, L. Ehm, S.M. Antao, P.L. Lee, P.J. Chupas, G. Liu, D.R. Strongin, M.A.A. Schoonen, B.L. Phillips, J.B. Parise, The Structure of Ferrihydrite, A Nanocrystalline Material, Science Express, May 24 2007. doi:10.1126/science.1142525, (Science Express Reports).

[21] J.M. Cowley, D.E. Janney, R.C. Gerkin, P.R. Buseck, The structure of ferritin cores determined by electron nanodiffraction, J. Struct. Biol. 131 (2000) 210–216.

[22] Y.G. Cheng, N.D. Chasteen, Role of phosphate in initial iron deposition in apoferritin, Biochemistry 30 (1991) 2947–2953 (and references therein).

[23] E.R. Bauminger, P.M. Harrison, Ferritin, the path of iron into the core, as seen by Mössbauer spectroscopy, Hyperfine Interact. 151/152 (2003) 3–19 (and references therein).

[24] E.R. Bauminger, P.M. Harrison, D. Hechel, N.W. Hudson, I. Nowik, A. Treffy, S.J. Yewdall, Iron(II) oxidation and early intermediates in iron-core formation in recombinant human H-chain ferritin, Biochem. J. 296 (1993) 709–719.

[25] P. Santambrogio, A. Cozzi, S. Levi, E. Rovida, F. Magni, A. Albertini, P. Arosio, Functional and immunological analysis of recombinant mouse H- and L-ferritins from *Escherichia coli*, Protein Expr. Purif. 19 (2000) 212–218.

[26] E.R. Bauminger, P. M Harrison, D. Hechel, I. Nowik, A. Treffry, Mössbauer spectroscopic investigation of structure-function relations in ferritins, Biochim. Biophys. Acta 1118 (1991) 48–58.

[27] S. Sun, N.D. Chasteen, Ferroxidase kinetics of horse spleen ferritin, J. Biol. Chem. 267 (1992) 25160–25166.

[28] E.L. Duarte, R. Itri, E. Lima Jr., M.S. Batista, T.S. Berquó, G.F. Goya, Large magnetic anisotropy in ferrihydrite nanoparticles synthesized from reverse micelles, Nanotechnology 17 (2006) 5549–5555.

[29] E. Murad, U. Schwertmann, The Mössbauer spectrum of ferrihydrite and its relation to those of other iron oxides, Am. Mineral. 65 (1980) 1043–1048.

[30] R.J. Pollard, C.M. Cardile, D.G. Lewius, L.J. Brown, Characterization of FeOOH polymorphs and ferrihydrite using low-temperature, applied-field Mössbauer spectroscopy, Clay Miner. 27 (1992) 57–71.

[31] L. Cianchi, F. Gulisano, G. Spina, Isotropic relaxation of the hyperfine field and intercluster interactions in ferrihydrite, J. Phys., Condens. Matter 6 (1994) 2269–2279.

[32] V.J. Wade, S. Levi, P. Arosio, A. Treffry, P.M. Harrison, S. Mann, Influence of site-directed modifications on the formation of iron cores in ferritin, J. Mol. Biol. 221 (1991) 1443–1452.

[33] T.G. St. Pierre, P. Chan, K.R. Bauchspiess, J. Webb, S. Betteridge, S. Walton, D.P.E. Dickson, Synthesis, structure and magnetic properties of ferritin cores with varying compositions and degrees of structural order: models for iron oxide deposits in iron-overload diseases, Coord. Chem. Rev. 151 (1996) 125–143.

[34] S. Mann, J.M. Williams, A. Treffy, P.A. Harrison, Reconstituted and native iron cores of bacterioferritin and ferritin, J. Mol. Biol. 198 (1987) 405–416.

[35] J.M. Williams, P.D. Danson, C. Janot, A Mössbauer determination of the iron core particle size distribution in ferritin, Phys. Med. Biol. 23 (1978) 835–851.

[36] K.S. Kaufman, G.C. Papaefthymiou, R.B. Frankel, A. Rosenthal, Nature of iron deposits on the cardiac walls in β-thalassemia by Mössbauer spectroscopy, Biochim. Biophys. Acta 629 (1980) 522–529.

[37] L. Néel, Theorie du trainage magnetique des ferromagnetiques en grains fins avec applications aux terres cuites, Ann. Geophys. 5 (1949) 99–136.

[38] W.F. Brown Jr., Thermal fluctuations of a single-domain particle, Phys. Rev. 130 (1963) 1677–1686; J. Appl. Phys. 34 (1963) 1319–1320;
The fundamental theorem of fine-ferromagnetic-particle theory, J. Appl. Phys. 39 (1968) 993–994.

[39] A. Aharoni, Relaxation processes in small particles, in: J.L. Dormann, D. Fiorani (Eds.), Magnetic Properties of Fine Particles, Elsevier Science, North-Holland, 1991, p. 3.

[40] D.P.E. Dickson, N.M.K. Reid, C. Hunt, H.D. Williams, M. El-Hilo, K. O'Grady, Determination of f_0 for fine magnetic particles, J. Magn. Magn. Mater. 125 (1993) 345–350.

[41] G. Liui, S. Debnath, K.W. Paul, W. Han, D.B. Hausner, H.-A. Hosein, F.M. Michel, J.B. Parise, D.L. Sparks, D.R. Strogin, Characterization and surface reactivity of ferrihydrite nanoparticles assembled in ferritin, Langmuir 22 (2006) 9313–9321.

[42] H. Gleiter, Materials with ultrafine microstructure: retrospectives and perspectives, Nanostruct. Mater. 1 (1992) 1–19.

[43] J.M. Coey, Noncollinear spin alignment in ultrafine ferrimagnetic crystallites, Phys. Rev. Lett. 27 (1971) 1140–1142.

[44] F.T. Parker, A.E. Berkowitz, Field response of surface spins on Co-adsorbed γ-Fe_2O_3, Phys. Rev., B 44 (1991) 7437–7443.
[45] G.J. Long, F. Grandjean (Eds.), Mössbauer Spectroscopy Applied to Magnetism and Materials Science, Plenum Press, New York, 1993.
[46] R.A. Brooks, J. Vymazal, R.B. Goldfarb, J.W. Bulte, P. Aisen, Relaxometry and magnetometry of ferritin, Magn. Reson. Med. 40 (1998) 227–235.
[47] R.B. Frankel, G.C. Papaefthymiou, G.D. Watt, Variation of superparamagnetic properties with iron loading in mammalian ferritin, Hyperfine Interact. 66 (1991) 71–82.
[48] J.K. Grady, Analytical Ultracentrifugation Studies of the Iron Distributions in Horse Spleen Ferritin, M.S. Thesis, University of New Hampshire, 1998, 68 pp.
[49] S. Mørup, H. Topsøe, Mössbauer studies of thermal excitations in magnetically ordered microcrystals, Appl. Phys. 11 (1976) 63–66.
[50] H. Kachkachi, E. Bonet, Surface-induced cubic anisotropy in nanomagnets, Phys. Rev., B 73 (2006) 224402–224409.
[51] H. Kachkachi, D.A. Garanin, Magnetic nanoparticles as many-spin systems, in: D. Fiorani (Ed.), Surface Effects in Magnetic Nanoparticles, Book Series in Nanostructure Science and Technology, Springer, US, 2005, pp. 75–104.